Resistive or Capacitive Charge-Division Readout for Position-Sensitive Detectors

Alberto Pullia, Walter F. J. Müller, Ciro Boiano, and Roberto Bassini

***Abstract*--Two-point charge division is a typical technique for position measurements in linear multi-electrode detectors (microstrips, multi-wire proportional counters, silicon drift-detector arrays, scintillators coupled to photodetectors). Only two preamplifiers, located at the right and the left ends of the detection array, are used, each of which receives a fraction of the charge produced by the ionizing event. Position is reconstructed comparing these charge fractions. In principle either a resistive or a capacitive divider may be used to split the charge. The choice between such two different setups is not obvious. In fact each of them shows advantages and disadvantages in terms of noise, signal propagation, linearity. In this paper we present a unified treatment for the capacitive and the resistive mechanisms of charge division which addresses the issues of this choice. As an example the realistic setup of the multi-wire position-sensitive proportional counter to be used in the TP-MUSIC III chamber of the ALADiN experiment at GSI is considered.**

I. Introduction

Two-point charge splitting is a measurement technique aimed at identifying the position of an ionizing event in linear multi-electrode detectors (Microstrips, Multi-Wire Proportional Counters (MWPC), Silicon Drift-Detector Arrays, Scintillators coupled to Segmented Photodetectors) [1], [2]. Rather than using an electronic channel per electrode, it makes use of only two "virtual-earth preamplifiers" with their virtual earths connected to the right and the left ends of the electrode array. Each preamplifier receives a fraction of the total charge produced by the event. The relative position x of the event along the array depends on these charge fractions, or :

$$\chi = \frac{x}{x_T} = \frac{Q_R}{Q_R+Q_L} \qquad (1)$$

where x_T is the total length of the array, Q_R is the charge collected at the right end point, Q_L is the charge collected at the left end point and the total charge Q_R+Q_L is used as a normalization factor. Both, either a resistive or a capacitive divider may be used to split the charge into fractions Q_L and Q_R, as is shown in the examples of Fig. 1. Each of these setups shows advantages and disadvantages in terms of noise, signal propagation, linearity, which depend on the constraints dictated by the detection system (capacitance and number of electrodes, required processing time, necessity of decoupling capacitors). In this paper a unified treatment for the capacitive and resistive mechanisms of the charge division is presented. The signal shape as well as the obtainable position resolution are derived vs. a suitable pattern of detector-processor parameters. It is found that the capacitive charge-division yields a higher resolution unless very short processing times are required. As an example the physical parameters of the MWPC of the TP-MUSIC III chamber installed at GSI are considered. This MWPC consists of a plane of anode wires (diameter=20 μm, 5 mm spacing) shielded from the detector volume by a Frisch grid located 5 mm far away. The Frisch grid acts as a gate that can be 'closed' when necessary, so as to prevent the slow positive ions produced in the multiplication volume from back scattering into the detector volume. The electrons traverse the region between the Frisch grid and the anode wires in 80-100 ns. The maximum time width of the

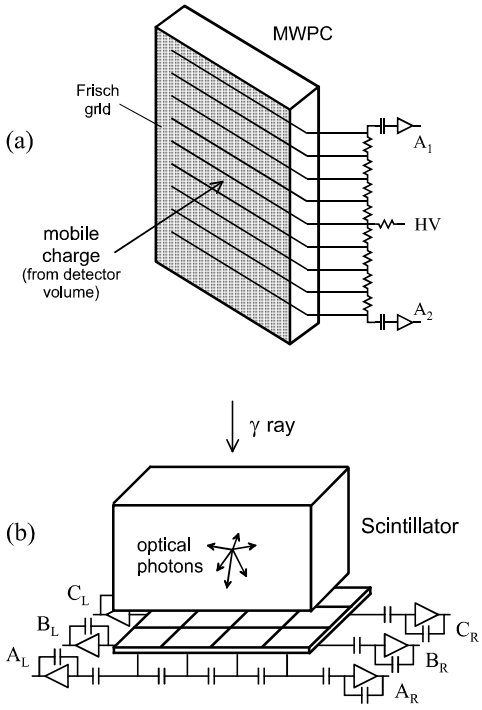

Fig. 1. Charge division in (a) a multi wire proportional counter and (b) a matrix of photodetectors coupled to a scintillator.

Manuscript received November 22, 2001. This work was supported by Italian INFN and MIUR, and German GSI.

A. Pullia is with the University of Milan, Department of Physics, and INFN Sez. di Milano, via Celoria 16, 20133 Milano - Italy (e-mail: alberto.pullia@mi.infn.it). W.F.J. Müller is with GSI, Abteilung KP3, D-64291 Darmstadt - Germany. C. Boiano and R. Bassini are with INFN Sez. di Milano, via Celoria 16, 20133 Milano - Italy.

charge cloud trespassing the Frisch grid, caused by thermal diffusion and/or by inclined trajectories of the primary ionizing particles, ranges between 20 to 150 ns, which sets a minimum for the processing time at about 200 ns. The shortest processing time is required in this application to maximize the resolving time in case of double or multiple hits in the detector volume.

An entirely different approach is based on terminating both ends of the charge-splitting line into the line characteristic impedance and use propagation times to derive the position. However such an approach is beyond the scopes of this paper

II. Signal propagation and nonlinearities

An electrical model of the charge-division line is shown in Fig. 2, where the electrode capacitances are drawn in dashed line. Signal is modeled as a short current pulse Qg(t) where Q is the collected charge and g(t) is a unit-area shape factor depending on the charge-collection mechanism. Decoupling capacitors C_d are also shown, while the high-value resistors used to bias the detector have been neglected. We want to calculate the current flowing into the virtual earths of the two far-end amplifiers as a function of the position of firing electrode. To do this let us model the network as the cascade of identical, symmetrical π-type cells of the type of those of Fig. 3, connected as shown in Fig. 4. Impedances Z_T terminating the line at both ends model the decoupling capacitors and the virtual earths. Virtual earths act as electronically cooled damping resistors [1], typically a few tens of ohms. These low-value resistors can be neglected in first approximation. C_w is the capacitance of the electrodes, R or C are the charge-splitting devices. Z_0 is the *characteristic impedance* of the cell, or the impedance seen at the input of a semi-infinite line (ℜ) of identical cells [3]. Parameter k is the so-called *transduction exponent* of the cell, defined as the natural logarithm of the input-to-output voltage ratio of each cell of such a line (ℜ) [3]. It can be shown that any symmetric cell is fully characterized by parameters Z_0 and k. After some calculations, shown in Appendices I.A and I.B, we derive

$$Z_0 = \begin{cases} \sqrt{\dfrac{R}{sC_w(1+¼sRC_w)}} \\ \dfrac{1}{s\sqrt{CC_w+¼C_w^2}} \end{cases} \qquad k = \begin{cases} \cosh^{-1}(1+½sRC_w) \\ \cosh^{-1}(1+½\dfrac{C_w}{C}) \end{cases} \tag{2}$$

for cells of Fig. 3(a) (first row of (2)) and (b) (second row of (2)). s is the independent variable in the Laplace domain. In Fig. 4 Z_1 and Z_2 are the impedances seen at the right/left side of the firing electrode. As is shown in Appendix I.C

$$Z_i = Z_0 \frac{Z_T \cosh n_i k + Z_0 \sinh n_i k}{Z_T \sinh n_i k + Z_0 \cosh n_i k} \tag{3}$$

where i=1,2. n_1 and n_2 are the cells located at the right /left side of the firing electrode. The signal current I_0 is split by current divider Z_1-Z_2, and flows thereafter through the line towards the far-end amplifiers. By using the current divider formula and Eq. (39) of Appendix I.C it is found that

$$I_{n1} = \frac{\cosh n_2 k + \dfrac{Z_0}{Z_T}\sinh n_2 k}{\left(\dfrac{Z_T}{Z_0}+\dfrac{Z_0}{Z_T}\right)\sinh nk + 2\cosh nk} I_0, \tag{4}$$

where indices 1 and 2 can be swapped and $n = n_1 + n_2$. If no

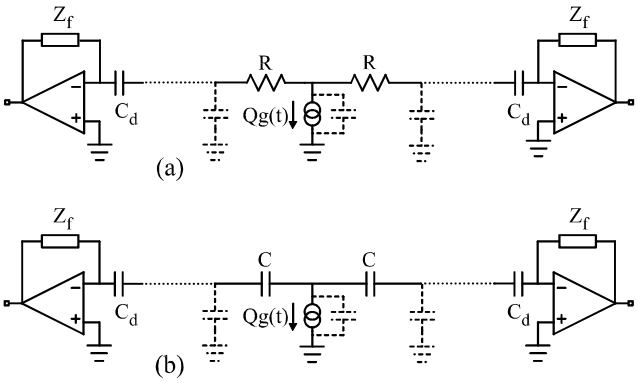

Fig. 2. Two-point measurement by means of (a) resistive divider (the stray capacitances in parallel to resistors R are neglected), (b) capacitive divider. The resistors R or capacitances C connect all detection elements to each other. Each detection element has a capacitive impedance to ground (capacitances in dashed line). The current signal delivered by the detector is Qg(t) where Q is the charge, unit-area function g(t) models the charge-collection mechanism. Decoupling capacitances C_d are also shown.

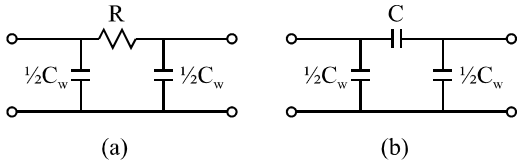

Fig. 3. Elementary cells by which the charge-division line may be modeled. C_w is the electrode (wire) capacitance. Elementary device for charge division is (a) a resistor R or (b) a capacitance C.

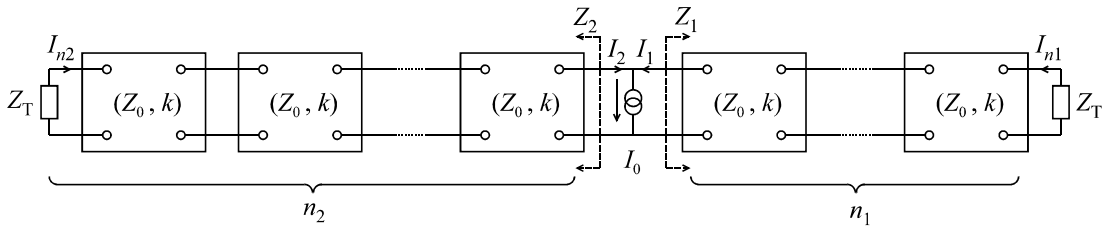

Fig. 4. Equivalent circuit of a charge-splitting line. Any cell models the charge-division element (a resistor or a capacitor) and the electrode impedance. The line is terminated into virtual earths of far-end amplifiers through coupling capacitors as modeled by impedances Z_T.

coupling capacitor is used Z_T vanishes and (3) and (4) become much simpler, namely

$$Z_i = Z_0 \tanh n_i k \,, \tag{5}$$

$$I_{n1} = \frac{\sinh n_2 k}{\sinh nk} I_0 \,. \tag{6}$$

Equations (4) and (6) show in the Laplace domain the propagation of the current signal from the firing electrode to the right-end amplifier. (4) and (6) hold namely when the line is terminated into the amplifier virtual earth through impedance Z_n or a short-circuit connection. Approximating g(t) as a delta-like impulse, I_0 becomes the Laplace transform of function Qδ(t), or I_0=L(Q$\delta(t)$)=Q. Inverse Laplace transform of (4) or (6) yields the current flowing into the amplifier virtual earth, which is clearly a function of n_2, or the position of the firing electrode.

A. Resistive divider

For the case of a resistive divider the first row of (2) holds. We search the time-domain counterparts of (4) and of (6) with Z_T=1/sC$_d$ and I_0=L(Q$\delta(t)$)=Q. To this purpose it is necessary to calculate the roots of the denominator of (4) and (6), or the poles of the network. After some calculations it turns out that the denominator of (4) may be rewritten as

$$\left(s\frac{\tau_w^2+4\tau_d^2}{4\tau_d}+\frac{C_w}{C_d}\right)\prod_{h=1}^{n-1}\left(s+\frac{4}{\tau_w}\sin^2\frac{h\pi}{2n}\right)+\tau_w\prod_{h=0}^{n-1}\left(s+\frac{4}{\tau_w}\sin^2\frac{2h+1}{4n}\pi\right) \tag{7}$$

where τ_d = RC$_d$, τ_w= RC$_w$. Apparently this polynomial is the sum of two polynomials, each with n known real roots, and has therefore n roots. Furthermore the roots of the overall polynomial are distinct and can be easily derived numerically. Similarly, the denominator of (6) may be rewritten as

$$\prod_{h=1}^{n-1}\left(s+\frac{4}{\tau_w}\sin^2\frac{h\pi}{2n}\right), \tag{8}$$

which apparently has n-1 distinct real roots. Whenever all poles are distinct, the inverse Laplace transform can be calculated using the well-known relationship:

$$L^{-1}\left\{\frac{N(s)}{D(s)}\right\}=\sum_r \frac{N(\alpha_r)}{D'(\alpha_r)}e^{\alpha_r t} \,, \tag{9}$$

where L^{-1} is inverse Laplace transform, α_r is the r-th root of D(s), the prime stands for derivative vs. s, t is time. We can use (9) to translate (4) (with Z_T=1/sC_d) in the time domain, being α_r the roots of (7). Similarly we can switch (6) in the time domain, obtaining, in this case exactly,

$$i_{n1}(t)=\frac{2Q}{n\tau_w}\sum_{r=1}^{n-1}(-1)^{r+1}\sin\frac{n_2 r\pi}{n}\sin\frac{r\pi}{n}e^{-\frac{4t}{\tau_w}\sin^2\frac{r\pi}{n}} \,. \tag{10}$$

Eq. (10) gives explicitly the current flowing into the virtual earth of far-end amplifier, when no decoupling capacitors are used, as a function of the position (dictated by n_2) of firing

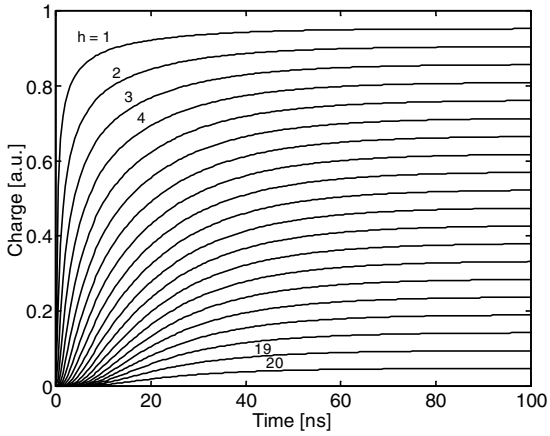

Fig. 5. Charge signal reaching one far-end amplifier in a proportional counter with 20 wires. Index h is position of the firing wire, in ascending order as the electrode gets further from the amplifier. R_{tot}=1.8kΩ, or R=90Ω. C_w=4.5pF. No decoupling capacitors are used. The waveforms stabilize after 100 ns.

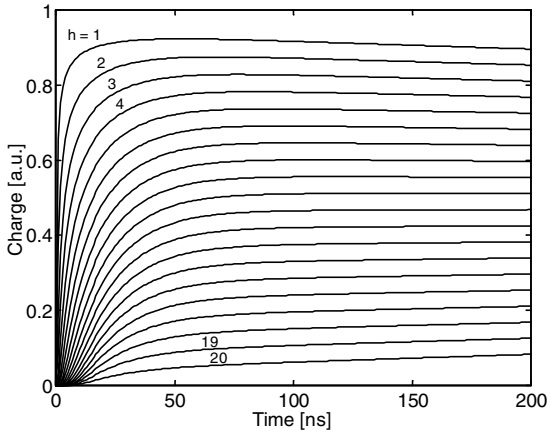

Fig. 6. Same as in Fig. 5 (20 electrodes, R=90Ω. Cw=4.5pF) but with decoupling capacitors of 2.2nF. Note the effect of decoupling capacitors: the waveforms never reach stable values.

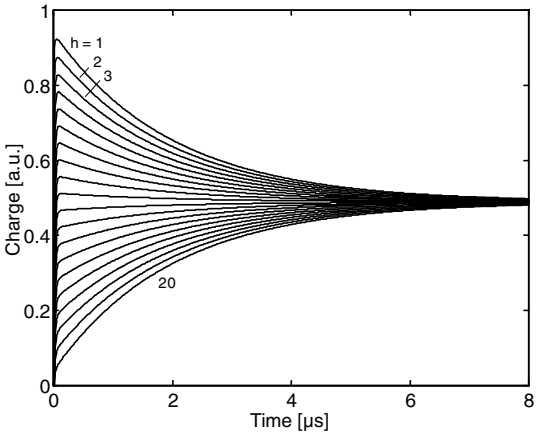

Fig. 7. Same as in Fig. 6, but on an expanded time scale. It can be seen that the waveforms decay exponentially converging to a common final level of about one half of the total collected charge Q (waveforms are normalized to Q in the figure). The time constant is dictated by the overall resistance of the divider and the series of the two decoupling capacitances, or 1.8 kΩ ×1.1 nF = 2 μs.

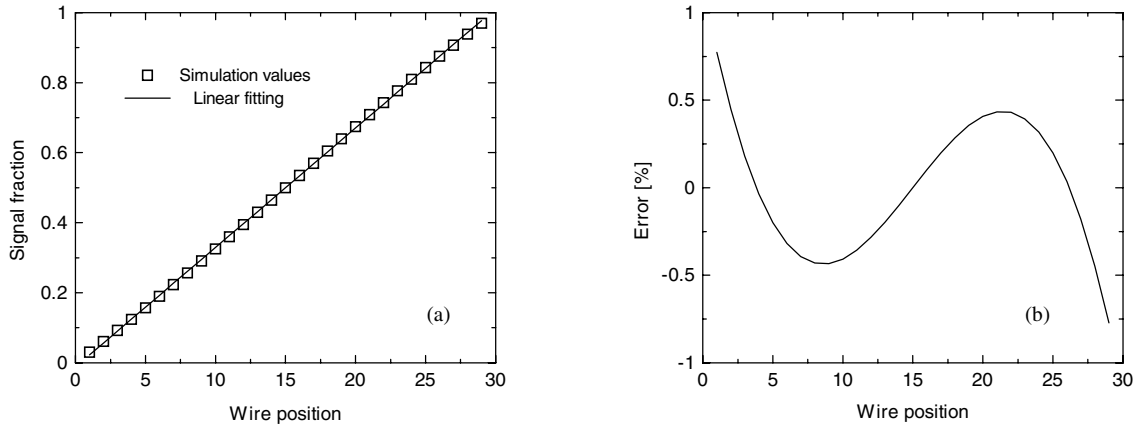

Fig. 8. Charge division with a capacitive-divider setup for a multi-wire proportional counter. Fraction (1) is reported vs the wire position while considering 29 wires. Wire capacitance is 0.8 pF. The capacitances C of the divider as well as C_d are of 1.1 nF. The nonlinearity is predicted to be <1%.

electrode. In Figs. 5-7 the integral of $i_{n1}(t)$, or the transmitted charge, is shown as normalized to the total collected charge Q for realistic values of the parameters. Note the effect of the decoupling capacitances in Figs. 6 and 7: the waveforms converge to a common final value of about one half of the total collected charge. This is rather intuitive: the collected charge cannot be eventually transmitted out of the resistor chain due to the decoupling capacitances which act as a barrier at low frequency. The charge will rather get redistributed on the large-value decoupling capacitors. This yields ½Q on each of the decoupling capacitances (assuming them equal to each other). It is worth pointing out that such a charge will be drained away in the long term by the high-value resistors used to bias the electrodes. Figs. 6 and 7 show clearly that if decoupling capacitors are used linearity will eventually depend on the shaping time constant. To address this problem sufficiently large decoupling capacitances are to be used, in such a way that the time constant of the charge redistribution process, or

$$(n\mathrm{R})\left(\tfrac{1}{2}\mathrm{C_d}\right) \tag{11}$$

is greater than the used shaping time. Alternatively a differentiator followed by a baseline restorer could be used to clip the slow tail caused by the decoupling capacitors.

The principal advantage of a resistive divider is a good linearity of the fraction (1) vs. position relationship. In fact at low frequency the electrode capacitances C_w behave as open-circuit connections and linearity is only limited by the accuracy of the divider resistors. This can be seen in Fig. 5: after ~100 ns linearly-distributed saturation values are reached. From a mathematical standpoint this can be seen in (6) where I_0=Q. If s vanishes, which corresponds to pushing t to infinity, then $k\rightarrow 0$ in (2), and (6) converges exactly to $\frac{n_2}{n}$Q. However capacitances C_w along with resistors R introduce phase shifts at high frequencies along the signal path, which yield a transient (noticeable for t<50 ns) and propagation delays (noticeable for t<15 ns) which get larger as the firing wire is further from the amplifier. To minimize such effects the resistor values should be chosen relatively low (90Ω in the shown examples). An empirical rule to determine the maximum transient duration (τ_0) is

$$\tau_0 \approx (n\mathrm{R})\left(\tfrac{1}{2}n\mathrm{C_w}\right), \tag{12}$$

which also permits to derive R as a function of the transient duration. As is shown in Appendix II.A (12) can be seen as the time constant of the line impedance as approximated at suitably low frequencies with a resistance (nR) and a capacitance (½nC$_w$) connected in parallel. Resistance nR is the series of n elementary resistors, capacitance ½nC$_w$ is one half of the parallel connection of all electrode capacitances C_w. Factor ½ arises because a voltage V supplied at one end of the line degrades to zero approaching the far end of the line and therefore the total charge stored on capacitances C_w is one half of V×nC$_w$. Low-value resistors should be used to make the transient (12) fast. The price to be paid for low-value resistors is a large amount of parallel current noise, as described in Sect. III.

B. Capacitive divider

For the case of a capacitive divider the second row of (2) holds. Note that in this case k is a constant and Z_0 is the impedance of a capacitance. Assume again I_0=Q. With these assumptions (4) with Z_T=1/sC$_d$ shows no dependence on s, and in consequence its time-domain counterpart is a delta-like function. This is not surprising: the line is a passive circuit made by capacitances only and has thus no bandwidth limitation. This is an advantage against the resistive-divider setup, in fact the transmitted charge, or the integral of $i_{n1}(t)$ is a clean step function. However the dependence of fraction (1) on position is non linear. In fact capacitances C_w sink small amounts of charge away from the main capacitive divider, which affects the linearity of the divider itself. In Fig. 8 the loss of linearity as derived from (6) is shown for realistic values of the parameters. To minimize this nonlinearity relatively large capacitances should be used in the divider. An empirical rule for such dimensioning is

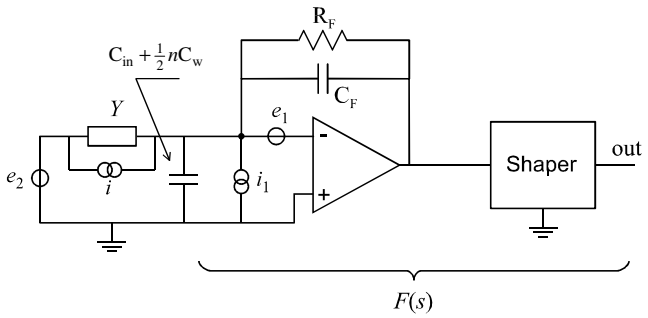

Fig. 9. Equivalent circuit of right-end amplifier and shaper useful for noise calculations. Swap indices 1 and 2 of noise sources to get the equivalent circuit of left-end amplifier.

$$\frac{\mathrm{C}}{n} > n\frac{\mathrm{C_w}}{2}, \tag{13}$$

in which a comparison is made between approximations of the charge stored onto the series of n capacitances C and that sunk away by capacitances $\mathrm{C_w}$, when an input voltage is given at one end of the divider, the factor ½ taking into account that the voltage on capacitances $\mathrm{C_w}$ degrades to zero approaching the far end of the line. The sum of the capacitances shown in (13) is a good approximation of the total line capacitance as is shown in Appendix II.B. If (13) is verified linearity will be mainly limited by the accuracy of the divider capacitors. Note that high-voltage capacitors should be used because typically thousands of volts are provided to bias the electrodes: if an electrode breaks down a fast-rising charge would be induced on the nearby capacitances and they could get damaged.

Advantages of a capacitive divider include a fast response and a low noise, as will be shown in Sect. III.

III. Noise of Position Figure

The complex impedance Z_n of the charge divider is the input load of the amplifiers, and is given by (46) and (48) of Appendices II.A and II.B, i.e.

$$Y_n = \frac{1}{Z_n} \approx s\tfrac{1}{2}n\mathrm{C}_w + Y \tag{14}$$

where from now on $s=\mathrm{j}\omega$, and

$$Y = \begin{cases} \dfrac{1}{n\mathrm{R}} & \text{(resistive divider)} \\ s\dfrac{\mathrm{C}}{n} & \text{(capacitive divider)} \end{cases} \tag{15}$$

Y_n has the form of a capacitance and a resistor in parallel (resistive divider) or of two capacitances in parallel (capacitive divider). Y represents the obvious component of Y_n inter-connecting the virtual earths of the two preamplifiers. The other component is associated to the electrode capacitances and can be visualized as a leakage path to ground. The Johnson noise (bilateral) associated to Y_n is

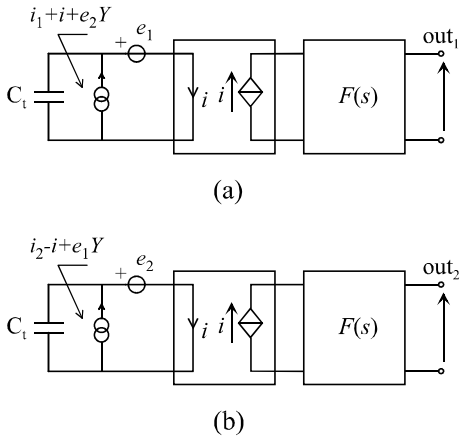

Fig. 10. Equivalent circuits of right-end (a) and left-end (b) amplifiers and shapers for noise calculations. A conventional direction is indicated for the instantaneous noise currents and voltages to highlight the correlations.

$$\overline{i^2} = 2KT\,\mathrm{Re}\{Y_n\}\delta f = \begin{cases} \dfrac{2KT}{n\mathrm{R}}\delta f = b_0\,\delta f & \text{(resistive divider)} \\ 0 & \text{(capacitive divider)} \end{cases} \tag{16}$$

where $\mathrm{Re}\{Y_n\}$ denotes the real component of Y_n, K is the Boltzmann constant, T is absolute temperature, and the other symbols are obvious. The principal noise sources at the right-end amplifier input are shown in Fig. 9, where noise injection from the opposite-end amplifier through path Y is apparent. In the left-end amplifier e_1 and i_1 must be replaced with e_2 and i_2 and e_2 with e_1. The following relations hold for the series and parallel noises (bilateral),

$$\begin{aligned} \overline{e_1^2} &= \overline{e_2^2} = 2KT\,\mathrm{R_S}\,\delta f = a\,\delta f \\ \overline{i_1^2} &= \overline{i_2^2} = \left(\frac{2KT}{\mathrm{R_F}} + qI_L\right)\delta f = b\,\delta f \end{aligned} \tag{17}$$

For an FET $\mathrm{R_S}=\alpha/g_\mathrm{m}$ where g_m is its transconductance and α is a constant factor ranging from 0.5 to 1 [4], and for a BJT $\mathrm{R_S}=1/2g_\mathrm{m}+R_{bb'}$ where $R_{bb'}$ is the base spreading resistor, $\mathrm{R_F}$ is the feedback resistor of the amplifier, q is the electronic charge, I_L the leakage current of the input transistor. In semiconductor detectors I_L should include an effective current obtained by summing all electrode's leakage currents each weighted linearly from 0 to 1 as the electrode position gets closer to the amplifier. Other non white noise contributions [5] have been neglected. $\mathrm{C_{in}}$ and $\mathrm{C_F}$ are the input and feedback capacitances of the amplifier. Note that the instantaneous Johnson-noise current (16) entering the right-end amplifier and that entering the left-end amplifier are anticorrelated. The series-noise cross talk through path Y introduces an additional correlation between the amplifiers' noises. These noise correlations must be taken into account in deriving the total noise of position figure (1). Figs. 10(a) and (b) show the equivalent circuits for noise analysis of the right- and the left-end amplifiers, where conventional signs are used for the instantaneous noise voltages and currents to highlight

their correlations. Appendix III shows how these equivalent circuits are derived. $F(s)$ is the Laplace transform of the impulse response $\mathrm{F}(t)$ of the amplifier-shaper chain normalized to its maximum value. Note that with such a normalization a current $\mathrm{Q}\delta(t)$ fed into the amplifier's virtual earth causes a signal at the shaper output with height Q.

Noise of position figure (1) in a bandwidth from f to $f+\delta f$ is given by the error propagation law, or

$$\overline{|d\chi|^2} = \left|\frac{\partial\chi}{\partial \mathrm{Q_R}}\right|^2 \overline{|d\mathrm{Q_R}|^2} + \left|\frac{\partial\chi}{\partial \mathrm{Q_L}}\right|^2 \overline{|d\mathrm{Q_L}|^2} + 2\,\mathrm{Re}\left\{\frac{\partial\chi}{\partial \mathrm{Q_R}}\frac{\partial\chi^*}{\partial \mathrm{Q_L}}\overline{d\mathrm{Q_R}\,d\mathrm{Q_R^*}}\right\} \tag{18}$$

where the star stands for complex conjugate, and

$$\begin{aligned} \mathrm{Q_R} &= h_2\mathrm{Q} \approx \frac{n_2}{n}\mathrm{Q} \\ \mathrm{Q_L} &= h_1\mathrm{Q} \approx \frac{n_1}{n}\mathrm{Q}\ . \end{aligned} \tag{19}$$

(18), (1) and (19) yield

$$\overline{|d\chi|^2} = \frac{h_1^2}{Q^2}\overline{|d\mathrm{Q_R}|^2} + \frac{h_2^2}{Q^2}\overline{|d\mathrm{Q_L}|^2} - 2\frac{h_1h_2}{Q^2}\mathrm{Re}\left\{\overline{d\mathrm{Q_R}\,d\mathrm{Q_R^*}}\right\}. \tag{20}$$

$d\mathrm{Q_R}$ and $d\mathrm{Q_L}$ are obtained from the equivalent circuits of Fig. 10 observing that the shaper output is read as an input-referred charge with the used normalization of $F(s)$:

$$\begin{aligned} d\mathrm{Q_R} &= i_1F(s) + iF(s) - e_1s\mathrm{C_t}F(s) + e_2YF(s) \\ d\mathrm{Q_L} &= i_2F(s) - iF(s) - e_2s\mathrm{C_t}F(s) + e_1YF(s) \end{aligned} \tag{21}$$

where e_1, e_2, i_1, i_2 are the instantaneous noise voltages and currents, $\mathrm{C_t}$ is the sum of all capacitances connected to the amplifier input, including the capacitive component of Y,

$$\mathrm{C_t} = \begin{cases} \mathrm{C_{in}} + \mathrm{C_F} + \frac{1}{2}n\mathrm{C_w} & \text{(resistive divider)} \\ \mathrm{C_{in}} + \mathrm{C_F} + \frac{1}{2}n\mathrm{C_w} + \dfrac{\mathrm{C}}{n} & \text{(capacitive divider)} \end{cases} \tag{22}$$

and so from (21)

$$\begin{aligned} \overline{|d\mathrm{Q_R}|^2} &= \left(\overline{i_1^2} + \overline{i^2} + \overline{e_2^2}|Y|^2 + \overline{e_1^2}\,|s\mathrm{C_t}|^2\right)|F(s)|^2 \\ \overline{|d\mathrm{Q_L}|^2} &= \left(\overline{i_2^2} + \overline{i^2} + \overline{e_1^2}|Y|^2 + \overline{e_2^2}\,|s\mathrm{C_t}|^2\right)|F(s)|^2 \\ \mathrm{Re}\left\{\overline{d\mathrm{Q_R}\,d\mathrm{Q_L^*}}\right\} &= -\left[\overline{i^2} + \left(\overline{e_1^2} + \overline{e_2^2}\right)\mathrm{C_t}\,\mathrm{Re}\left\{sY^*\right\}\right]|F(s)|^2 \end{aligned} \tag{23}$$

In (23) the mean squared voltages and currents are given by (16) and (17), Y is given by (15), and $\mathrm{C_t}$ by (22). Putting (23) in (20) and integrating over all values of f (from -∞ to ∞) one obtains the variance σ_χ^2 of the position figure. Frequency dependence of (23) is dictated by factors $|F(j\omega)|^2$ or $\omega^2|F(j\omega)|^2$. The integral of such factors over the frequency is often translated in the time domain thanks to Parseval's theorem [6], [7], or

$$\begin{aligned} \int_{-\infty}^{\infty}\omega^2|F(j\omega)|^2\,df &= \int_{-\infty}^{\infty}|\mathrm{F}'(t)|^2\,dt = \frac{A}{\mathrm{T_P}} \\ \int_{-\infty}^{\infty}|F(j\omega)|^2\,df &= \int_{-\infty}^{\infty}|\mathrm{F}(t)|^2\,dt = B\,\mathrm{T_P} \end{aligned} \tag{24}$$

where the prime stands for time derivative. $\mathrm{T_P}$ is the "time width parameter" of $\mathrm{F}(t)$ or the "processing time" and A, B are nondimensional form factors depending on the shape of $\mathrm{F}(t)$ and not on its time scale. Numerical values of A, B are listed for most cases in [8].

Case of resistive divider: Putting (23) with $Y=1/n\mathrm{R}$ in (20) and integrating over f with the help of (24) one thus obtains

$$\sigma_{\chi\mathrm{R}}^2 = \frac{1}{\mathrm{Q}^2}\left[\psi\, a\mathrm{C_{tR}^2}\,\frac{A}{\mathrm{T_P}} + (\psi\, b + b_0)B\,\mathrm{T_P}\right] \tag{25}$$

where second index "R" denotes the resistive-divider case and $\psi = h_1^2 + h_2^2$ is a factor depending on the position of charge injection. Taking into account that (19) yield $h_1+h_2=1$ one obtains $\psi = 2h_1^2 - 2h_1 + 1$. ψ is plotted vs. h_1 in Fig. 11. It is worth noting that the dependence of (25) on ψ tends to vanish if the noise component $b_0 B\,\mathrm{T_P}$ brought about by the resistive divider, see (16), dominates over the others. This is rather intuitive: in this case the noises seen at the output of the amplifiers are anticorrelated and the noise of the sum is much lower than the noise of individual ends. Therefore the error in the position figure (1) is dictated by the noise of one amplifier only and it is thus independent of the location of the charge injection.

Case of capacitive divider: Putting (23) with $Y=s\mathrm{C}/n$ in (20) and integrating over f with the help of (24) one obtains

$$\sigma_{\chi\mathrm{C}}^2 = \frac{1}{\mathrm{Q}^2}\left[\left(\psi + \frac{2-\psi}{n^2}\frac{C^2}{\mathrm{C_{tC}^2}}\right)a\mathrm{C_{tC}^2}\,\frac{A}{\mathrm{T_P}} + \psi\, bB\,\mathrm{T_P}\right] \tag{26}$$

where second index "C" denotes the capacitive-divider case. It is worth noting that the dependence of (26) on ψ tends again to vanish if $\mathrm{C_{tC}}$ is dominated by the capacitive divider, i.e. $\mathrm{C_{tC}}\approx\mathrm{C}/n$, and the series-noise component $a\mathrm{C_{tC}^2}A/\mathrm{T_P}$ dominates. In this case the cross talk between series noises makes the noises at the preamplifiers' outputs again anticorrelated, so that the noise of the sum is much lower than the noise of individual ends. Therefore the error in the position figure (1) is dictated by the noise of one amplifier only and is thus independent of the location of the charge injection.

A comparison between resistive- and capacitive-divider setups translates into a comparison of the variances (25) and (26). The ratio between variances (26) and (25) is

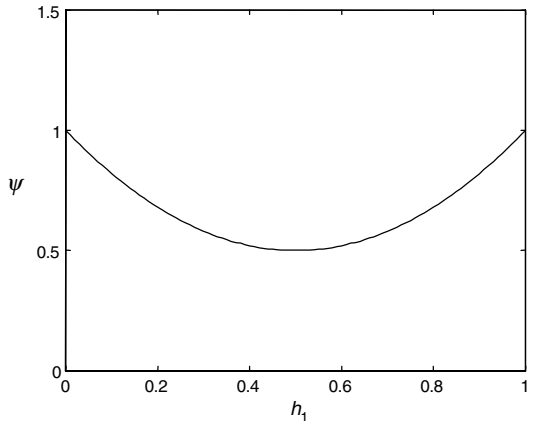

Fig. 11. Factor ψ vs. $h_1=n_1/n$. ψ ranges from 0.5 to 1 depending on the position of charge injection (from the middle of the array to the end points).

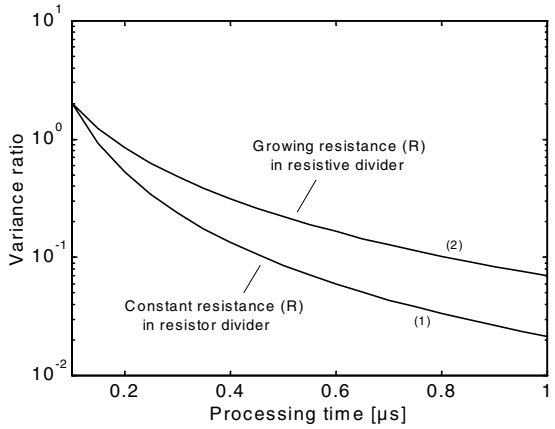

Fig. 12. Ratio of the variances of the position estimate for capacitive- and resistive-divider setups in a 20 wire (C_w=4.5 pF) MWPC with Frisch grid. Parameters: g_m=10 mS, C_{in}=10 pF. C_F=10 pF. Capacitive divider: C_{tC}=285 pF, R_F=50 MΩ, I_L=0.5 nA. Resistive divider: C_{tR}=65 pF, nR=1.8 kΩ, R_F=6 kΩ, I_L=0.5 nA.

$$r_{CR}^2 = \frac{\sigma_{\chi C}^2}{\sigma_{\chi R}^2} = \frac{\left(\psi + \frac{2-\psi}{n^2}\frac{C^2}{C_{tC}^2}\right) a C_{tC}^2 \frac{A}{T_P} + \psi\, bB\, T_P}{\psi\, a C_{tR}^2 \frac{A}{T_P} + (\psi\, b + b_0) B\, T_P}, \quad (27)$$

which apparently depends on the processing time T_P. The resistive divider enhances the parallel noise (current noise of resistor nR) and the capacitive divider enhances the series noise (capacitance C/n enhances the total input capacitance C_{tC}). We so expect that the resistive divider has a better performance at short processing times and the opposite for the capacitive divider. However a resistive setup with nR in the kohm range typically enhances the parallel-noise contribution by several orders of magnitudes with respect to capacitive setups, while a capacitive setup with C/n ranging from 50 pF to 500 pF typically increases the series-noise contribution by one order of magnitude with respect to resistive setups. We thus expect that in most cases capacitive charge division yields a higher resolution than resistive division at the optimum processing times.

As an example, consider a MWPC of the type of that of Fig. 1(a) with 20 wires having C_w=4.5 pF (½nC_w=45 pF), and two possible dividers: the first made by 20 resistors of 90 Ω each (nR=1.8 kΩ), the second made by 20 capacitances of 4.4 nF (C/n=220 pF) each. For both cases the amplifier's input transistor has a capacitance C_{in}=10 pF and a transconductance g_m=10 mS. I_L is assumed 0.5 nA, and a symmetrical trapezoidal shaper amplifier with a flat-top to base ratio of 1/3 is used (A=2, B=1.67). In Fig. 12, curve (1), r_{CR}^2 is shown where the above mentioned parameters are used, ψ=1, and the "processing time" is the width of the sloped edge of the trapezoid. Larger-than-unity values on the y-axis indicate convenience for resistive against capacitive divider, and viceversa. Curve (2) has been obtained by increasing R proportionally to the processing time. In fact the divider's resistance is a tradeoff between the transient time of the RC_w line and the parallel noise. If R is proportional to the processing time the transient time will be always an acceptable fraction of the processing time itself and parallel noise will be not as high at longer processing times. Curves (1) and (2) do not change noticeably by varying ψ in the 0.5 to 1 range. It can be seen that for very fast processing times, shorter than ≈200 ns in the considered case, the resistive divider may yield a lower noise. At a processing time of 1 μs, however, the capacitive divider yields one-to-two orders of magnitude of lower noise.

It is worth pointing out that with an array of photodetectors coupled to a scintillator the charge-collection mechanism would be in the μs range, and therefore the noise analysis should be made at much longer processing times than in Fig. 12. In this case a capacitive-divider setup would be more adequate.

A very simple system consisting of a discrete network of resistors and capacitors, custom-made charge amplifiers, and quasi-Gaussian shaper amplifiers has been arranged to check the shown theory. The observed signals and noise have been found in good agreement with (10), (25) and (26).

A different position figure, or

$$\frac{Q_R - Q_L}{Q_R + Q_L}, \quad (28)$$

is sometimes used rather than (1). (28) ranges from -1 to 1 rather than from 0 to 1, thus the signal swing gets doubled. However the squared noise of such figure, as obtained with the same procedure used to derive (25) and (26), is found to be four times as large. Therefore (28) has the same signal-to-noise ratio as (1). The shown analysis holds for both of them.

IV. Conclusion

The principal advantage of a resistive divider is the potentially good linearity of position figure vs. position relationship. The price to be paid is a large amount of parallel noise. Such noise contribution decreases as the processing time is decreased. However the processing time should be greater than the time transient due to phase shifts in the RC_w line and the intrinsic signal width caused by the charge collection mechanism.

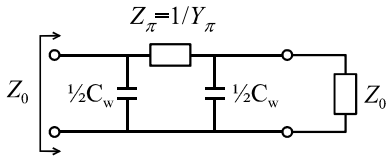

Fig. 13. Equivalent circuit for calculation of the characteristic impedance.

The principal advantages of a capacitive divider, instead, are a fast response and a low noise. However the dependence of position figure vs. position in this case is non linear. To minimize such nonlinearity large-value capacitances should be used in the divider. However these capacitances cannot be chosen too large because the series noise of the preamplifier is enhanced as the input capacitance is increased. A correct dimensioning of the divider capacitance appears as a trade off between nonlinearity and noise.

A unified method to derive the waveforms and the noise of the two configurations has been presented and discussed and indications for a correct dimensioning of the setups have been shown. A possible development of the method consists of including 1/*f*- and Lorentzian-noise components in the amplifiers' series noise.

V. Appendices

I.A. Calculation of characteristic impedance Z_0

Z_0 is the input impedance of a semi-infinite line of identical cells. Let us connect a semi-infinite line of cells, as modeled by Z_0, to the output of an individual cell of the same type, as shown in Fig. 13.

The input impedance of such cell is again Z_0. By calculating it on the circuit of Fig. 13 one obtains the following identity (call $Y_0=1/Z_0$):

$$Y_0 = \tfrac{1}{2} s\mathrm{C_w} + \frac{Y_\pi \left(Y_0 + \tfrac{1}{2} s\mathrm{C_w}\right)}{Y_\pi + Y_0 + \tfrac{1}{2} s\mathrm{C_w}}. \tag{29}$$

Solving (29) for Y_0 one obtains

$$Y_0^2 = s\mathrm{C_w}\left(Y_\pi + \tfrac{1}{4} s\mathrm{C_w}\right) \tag{30}$$

Putting Y_π=1/R or Y_π=*s*C in (30) yields the first column of (2).

I.B. Calculation of transduction exponent k

Connect a voltage source V_{in} to the input of the cell of Fig. 13. Let us calculate the output voltage of this cell:

$$V_{out} = \frac{Y_\pi}{Y_\pi + Y_0 + \tfrac{1}{2} s\mathrm{C_w}} V_{in} \tag{31}$$

Using Y_0 as given by (30) in (31) we find

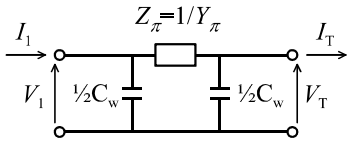

Fig. 14. Elementary π-type symmetric cell.

$$\frac{V_{in}}{V_{out}} = 1 + \frac{s\mathrm{C_w}}{2Y_\pi} + \sqrt{\left(1 + \frac{s\mathrm{C_w}}{2Y_\pi}\right)^2 - 1} \tag{32}$$

and hence

$$k = \ln\left(\frac{V_{in}}{V_{out}}\right) = \cosh^{-1}\left(1 + \frac{s\mathrm{C_w}}{2Y_\pi}\right) \tag{33}$$

Putting Y_π=1/R or Y_π=*s*C in (33) yields the second column of (2).

I.C. Equations for the series connection of n cells

Consider the cell of Fig. 14. The relations

$$\begin{cases} V_1 = V_\mathrm{T}\left(1 + \tfrac{1}{2} sZ_\pi \mathrm{C_w}\right) + I_\mathrm{T} Z_\pi \\ I_1 = V_\mathrm{T}\left(\tfrac{1}{4} s^2 Z_\pi \mathrm{C_w^2} + s\mathrm{C_w}\right) + I_\mathrm{T}\left(1 + \tfrac{1}{2} sZ_\pi \mathrm{C_w}\right) \end{cases} \tag{34}$$

hold. Using (30) and (33) with $Y_\pi=1/Z_\pi$, (34) become

$$\begin{cases} V_1 = V_\mathrm{T} \cosh k + I_\mathrm{T} Z_0 \sinh k \\ I_1 = V_\mathrm{T} \dfrac{\sinh k}{Z_0} + I_\mathrm{T} \cosh k \end{cases} \tag{35}$$

Now let us connect a second identical cell at its input and call V_2 and I_2 the voltage and the current at the input of the second cell. Similarly to (35)

$$\begin{cases} V_2 = V_1 \cosh k + I_1 Z_0 \sinh k \\ I_2 = V_1 \dfrac{\sinh k}{Z_0} + I_1 \cosh k \end{cases} \tag{36}$$

and substituting (35) in (36) we obtain

$$\begin{cases} V_2 = V_\mathrm{T} \cosh 2k + I_\mathrm{T} Z_0 \sinh 2k \\ I_2 = V_\mathrm{T} \dfrac{\sinh 2k}{Z_0} + I_\mathrm{T} \cosh 2k \end{cases} \tag{37}$$

Generalising (37) for *n* cells

$$\begin{cases} V_n = V_\mathrm{T}\cosh nk + I_\mathrm{T} Z_0 \sinh nk \\ I_n = V_\mathrm{T}\dfrac{\sinh nk}{Z_0} + I_\mathrm{T}\cosh nk \end{cases} \tag{38}$$

Putting a terminating impedance $Z_\mathrm{T}=V_\mathrm{T}/I_\mathrm{T}$ at the end of the line and calculating the ratio between the first and the second of (38) yields (3).

Furthermore dividing the second of (38) by I_T yields the useful relation

$$\frac{I_\mathrm{T}}{I_n} = \frac{1}{\dfrac{Z_\mathrm{T}}{Z_0}\sinh nk + \cosh nk} \tag{39}$$

II.A. Impedance of an n-cell resistive line at low frequency

Consider the cascade of n cells of the type shown in Fig. 3(a), short circuited at the far end. The impedance of such line is given by (5) and (2). Let us develop the hyperbolic tangent term in (2):

$$\begin{aligned} \tanh nk &= \tanh n\cosh^{-1}(1+\tfrac{1}{2}s\tau_\mathrm{w}) = \\ &= \tanh \ln\left[1+\tfrac{1}{2}s\tau_\mathrm{w} + \sqrt{\left(1+\tfrac{1}{4}s\tau_\mathrm{w}\right)^2 - 1}\right]^n = \\ &= \frac{(1+x)^n - (1+x)^{-n}}{(1+x)^n + (1+x)^{-n}} \end{aligned} \tag{40}$$

where

$$x = \tfrac{1}{2}s\tau_\mathrm{w} + \sqrt{s\tau_\mathrm{w}\left(1+\tfrac{1}{4}s\tau_\mathrm{w}\right)}. \tag{41}$$

Expanding terms $(1+x)^n$ and $(1+x)^{-n}$ in (40) yields

$$\tanh nk \approx \frac{nx}{1+\tfrac{1}{2}n^2x^2} \tag{42}$$

Putting $s = j\omega$ in (41) and assuming suitably low frequencies

$$\omega << 1/\tau_\mathrm{w}, \tag{43}$$

(41) yields

$$x \approx \sqrt{s\tau_\mathrm{w}\left(1+\tfrac{1}{4}s\tau_\mathrm{w}\right)}. \tag{44}$$

Substituting (44) in (42) yields

$$\tanh nk \approx \frac{n\sqrt{s\tau_\mathrm{w}\left(1+\tfrac{1}{4}s\tau_\mathrm{w}\right)}}{1+\tfrac{1}{2}n^2 s\tau_\mathrm{w}\left(1+\tfrac{1}{4}s\tau_\mathrm{w}\right)} \tag{45}$$

Substituting (45) and (2) in (5) yields the low-frequency impedance Z_n of the n-cell line, or

$$Y_n = \frac{1}{Z_n} \approx \frac{1}{n\mathrm{R}} + \frac{ns\mathrm{C}_\mathrm{w}}{2}. \tag{46}$$

This is the parallel connection of an equivalent resistor nR and an equivalent capacitor $\frac{1}{2}n\mathrm{C}_\mathrm{w}$. (46) is an acceptable approximation, in fact the processing time must be greater than (12), which yields (43).

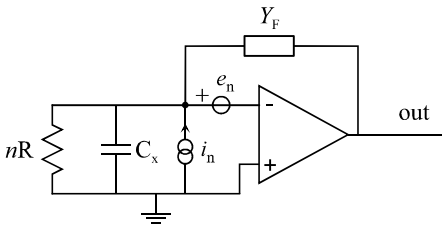

Fig. 15. Circuit for noise analysis.

II.B. Impedance of an n-cell capacitive line

Consider the cascade of n cells of the type shown in Fig. 3(b), short circuited at the far end. The impedance of such line is given by (5) and (2). A procedure similar to that of Appendix II.A where R is substituted with $1/s$C can be used to simplify (5). Instead of (43) we thus pose

$$\frac{\mathrm{C}}{\mathrm{C}_\mathrm{w}} >> 1 \tag{47}$$

and we finally get

$$Y_n = \frac{1}{Z_n} \approx \frac{s\mathrm{C}}{n} + \frac{ns\mathrm{C}_\mathrm{w}}{2} \tag{48}$$

The line impedance as expected is a pure capacitance, but two simple contributions are now put into evidence. (48) is an acceptable approximation, in fact (13) yields (47).

III. Equivalent circuit for noise calculations

Consider the circuit of Fig. 15 in which $Z_\mathrm{F}=1/Y_\mathrm{F}$ is the impedance of a capacitance $\mathrm{C_F}$ in parallel with a resistor $\mathrm{R_F}$,

$$\frac{1}{Z_\mathrm{F}} = Y_\mathrm{F} = s\mathrm{C_F} + \frac{1}{\mathrm{R_F}} \tag{49}$$

and e_n, i_n are the instantaneous voltage and current noises. Let us propagate e_n and i_n to the output:

$$\begin{aligned} V_{o1} &= e_\mathrm{n}\frac{\dfrac{1}{\mathrm{R_F}} + \dfrac{1}{n\mathrm{R}} + s(\mathrm{C_x}+\mathrm{C_F})}{Y_\mathrm{n}} \\ V_{o2} &= -i_\mathrm{n}\frac{1}{Y_\mathrm{n}} \end{aligned} \tag{50}$$

V_{o1} and V_{o2} are the individual contributions of e_n and i_n to the output. $\mathrm{C_x}$ is the capacitive component of the input impedance. We now want to refer the first of (50) to an equivalent input current. To this purpose we equal the first of (50) to the second where i_n is substituted with the wanted equivalent current i_eq. This yields

$$i_{eq} = -e_n\left(\frac{1}{R_F}+\frac{1}{nR}\right)-e_n sC_t \qquad (51)$$

The overall equivalent noise current i_T flown into the amplifier virtual earth is so

$$i_T = i_n - e_n\left(\frac{1}{R_F}+\frac{1}{nR}\right)-e_n sC_t = i_n - i_{en} - e_n sC_t\,. \qquad (52)$$

(52) shows that the principal system noises may be referred to the input by means of a unique noise current source injecting noise into the amplifier virtual earth. (52) contains a term $e_n sC_t$ that can be conveniently visualized as a voltage source e_n injecting a current into the amplifier virtual earth through a capacitor $C_t=C_x+C_F$. The other components of the current noise source (52) have spectral densities (bilateral)

$$\frac{\overline{i_n^2}}{\delta f} = \frac{2KT}{nR}+\frac{2KT}{R_F} \qquad (53)$$

$$\frac{\overline{i_{en}^2}}{\delta f} = 2KTR_S\left(\frac{1}{R_F}+\frac{1}{nR}\right)^2. \qquad (54)$$

where R_S, or the series-noise equivalent resistor, is discussed after Eq. (17). It can be shown that (53) dominates over (54) if

$$R_S < \frac{nRR_F}{nR+R_F} \qquad (55)$$

which is largely met in most cases, being R_S a few tens of ohms typically. We conclude that (52) yields in good approximation

$$i_T \approx i_n - e_n sC_t \qquad (56)$$

or the sum of two uncorrelated components. Note that the sign "-" in (56) is not important being e_n and i_n uncorrelated. (56) is visualized by means of an equivalent circuit of the type of those shown in Fig. 10.

VI. Acknowledgments

The authors gratefully thank E. Gatti, P. Rehak, and I. Iori for fruitful discussions.

VII. References

[1] V. Radeka, "Position sensitive semiconductor detectors signal formation, noise and position readout," Proc. of Workshop on Silicon Detectors for High Energy Physics, Fermilab 15-16 Oct. 1981, p. 21.

[2] R. B. Owen, M. L. Awcock, "One and two dimensional position sensing semiconductor detectors," IEEE Trans. Nucl. Sci., vol. 15, pp. 290-303, 1968.

[3] A. Ghizzettti, *Calcolo simbolico*. Bologna: N. Zanichelli, 1943, pp. 239-242.

[4] A. Van Der Ziel, "Noise in solid-state devices and lasers," *Proc. IEEE*, vol. 58, no. 8, pp. 1178-1206, 1970.

[5] P.F. Manfredi, "New perspectives in low noise preamplifier design for room temperature X-ray detectors," in *Semiconductor for Room-Temperature Radiation Detector Applications*, Proceedings of the Material Research Society 1993 Spring Meeting, S. Francisco, CA, April 12-16, pp. 213-223, 1993.

[6] F. S. Goulding, "Pulse shaping in low-noise nuclear amplifiers: a physical approach to noise analysis," *Nucl. Instr. Meth.*, vol. 100, pp. 493-504, 1972.

[7] V. Radeka,"Optimum signal processing for pulse-amplitude spectrometry in the presence of high-rate effects and noise," *IEEE Trans. Nucl. Sci.*, vol. 15, no. 3, pp. 455-481, 1968.

[8] E. Gatti, P.F. Manfredi, M. Sampietro, V. Speziali, "Suboptimal filtering of 1/*f*-noise in detector charge measurements," *Nucl. Instr. and Meth.*, vol. A297, pp. 467-478, 1990.